




Ferroelectric domain architecture and poling of BaTiO₃ on Si

Journal Article

Author(s):

[Nordlander, Johanna](#) ; [Eltes, Felix](#); [Reynaud, M.](#); [Nürnberg, Jacob](#); [De Luca, Gabriele](#); [Caimi, Daniele](#); [Demkov, Alexander A.](#); [Abel, Stefan](#); [Fiebig, Manfred](#) ; [Fompeyrine, Jean](#); [Trassin, Morgan](#) 

Publication date:

2020-03

Permanent link:

<https://doi.org/10.3929/ethz-b-000408059>

Rights / license:

[In Copyright - Non-Commercial Use Permitted](#)

Originally published in:

Physical Review Materials 4(3), <https://doi.org/10.1103/PhysRevMaterials.4.034406>

Funding acknowledgement:

694955 - In-situ second harmonic generation for emergent electronics in transition-metal oxides (EC)

178825 - Dynamical processes in systems with strong electronic correlations (SNF)

780997 - Wafer-scale, CMOS integration of photonics, plasmonics and electronics for mass manufacturing 200Gb/s NRZ transceivers towards low-cost Terabit connectivity in Data Centers (EC)

159565 - Plasmonic Active Devices based on Metal Oxides (SNF)

Ferroelectric domain architecture and poling of BaTiO₃ on Si

J. Nordlander^{1,*}, F. Eltes², M. Reynaud³, J. Nürnberg¹, G. De Luca^{1,4}, D. Caimi,²
A. A. Demkov³, S. Abel², M. Fiebig¹, J. Fompeyrine² and M. Trassin^{1,†}

¹Department of Materials, ETH Zurich, 8093 Zurich, Switzerland

²IBM Research–Zurich, 8803 Rüschlikon, Switzerland

³Department of Physics, The University of Texas at Austin, Austin, Texas 78712, USA

⁴Department of Physics, University of Zurich, 8057 Zurich, Switzerland



(Received 5 November 2019; accepted 18 February 2020; published 18 March 2020)

We investigate the ferroelectric domain architecture and its *operando* response to an external electric field in BaTiO₃-based electro-optic heterostructures integrated on silicon. By noninvasive optical second-harmonic generation, we identify the preexistence of in-plane (*a*-) domains dispersed within a predominantly out-of-plane- (*c*-) oriented matrix. Monitoring the poling behavior of the respective domain populations, we show that the spontaneous polarization of these *a*-domains lack a predominant orientation in the pristine state, yet can be selectively aligned with an in-plane electric field, leaving the *c*-domain population intact. Hence, domain reorientation of a ferroelastic *c*-to-*a* type was directly excluded. Such independent electrical control of ferroelectric *a*-domains in a *c*-oriented BaTiO₃ film on silicon is a valuable platform for engineering multidirectional electro-optic functionality in integrated photonic devices.

DOI: [10.1103/PhysRevMaterials.4.034406](https://doi.org/10.1103/PhysRevMaterials.4.034406)

I. INTRODUCTION

Ferroelectric materials host a range of properties of great technological relevance: their inherent piezoelectric effect motivated their original use as mechanical elements in, e.g., sensors or actuators, and the electric-field controllability of their spontaneous polarization has placed them as key elements for oxide electronics [1,2]. Ferroelectric materials also exhibit characteristic optical properties that extend their device potential to the field of photonics [3–6]. In particular, the pronounced linear electro-optic effect (Pockels effect) exhibited by some ferroelectrics allows energy-efficient control of light propagation through tuning of the refractive index n proportional to an external electric field E^{ext} , that is, $\Delta n_{ij} \propto r_{ijk} E_k^{\text{ext}}$. The Pockels tensor components r_{ijk} parametrize the strength of the effect and relate it to the noncentrosymmetric crystal structure of the material. In ferroelectrics, the electro-optic properties are thus closely connected to their ferroelectric domain configuration, that is, the spatial distribution of the inversion-symmetry-breaking spontaneous polarization.

The many technological prospects of combining such electro-optic ferroelectrics with the established silicon-based electronics platform has been a major driving force for the integration of epitaxial ferroelectric thin films on silicon substrates [7–9]. One of the most prominent ferroelectrics used for this implementation is BaTiO₃ (BTO), by virtue of being lead-free in addition to exhibiting exceptionally high Pockels coefficients at typical telecommunication wavelengths, like 1310 and 1550 nm [6]. However, strain relaxation effects accompanying the BTO thin-film growth directly on SrTiO₃ (STO)-buffered silicon for electro-optic applications,

excluding the insertion of additional buffer layers [10–12], usually result in a complex domain architecture [13,14]. The spontaneous polarization in BTO films on silicon (BTO | Si) may point along the out-of-plane or either of the two in-plane, principal crystallographic axes. In particular, a mixture of nanoscale domains, each with polarization along one of these three directions, is often observed [15]. The superposition of electro-optic effects specific to each of these domain states in a multidomain sample results in a highly nontrivial electro-optic behavior at the macroscopic level of the device. Hence, characterizing the domain distribution and its response to applied electric fields is crucial for understanding and controlling the optical properties of the ferroelectric layer. This remains challenging, however, in a device heterostructure. So far, probing the polarization state of BTO | Si has mainly been restricted either to invasive characterization such as transmission electron microscopy or to scanning probe techniques [15–18], which are sensitive to surface information only. Direct access to the domain architecture of BTO | Si as it evolves with applied electric fields in the active volume of an electro-optic device requires a simultaneously nondestructive and bulk-sensitive probe technique that, on top of all this, has to be applicable *operando*, that is, during electric-field operation of the device.

Here, we used spatially resolved optical second-harmonic generation (SHG) to characterize the ferroelectric domain distribution noninvasively and throughout the thickness of BTO thin films on silicon. This method allowed us to distinguish between the individual domain states in a multidomain architecture, including, in particular, the detection of disordered as-grown *a*-domains within a *c*-oriented matrix. Monitoring the evolution of *a*- and *c*-domain populations in response to an in-plane electric field in an *operando* approach further allowed us to determine details of the in-plane poling mechanism. We found that the alignment of *a*-domains occurs

*johanna.nordlander@mat.ethz.ch

†morgan.trassin@mat.ethz.ch

purely through in-plane domain reorientation, without any occurrence of ferroelastic c - to a -domain transformation, so that the c -domain population remains intact during the poling.

II. THIN FILM GROWTH AND STRUCTURE

Our electro-optic heterostructure, a 50-nm ferroelectric BTO thin film on STO-buffered (001)-oriented silicon, was grown using molecular beam epitaxy (MBE) as described in Ref. [7]. The orientation of the macroscopic polarization of BTO on STO-buffered silicon is controlled by the thickness-dependent strain relaxation of the BTO layer [14]. The epitaxial relationship between the substrate and the tetragonal BTO thin film was confirmed with x-ray diffraction (Fig. 1). The two a axes lie in the plane of the BTO film, $[110]_{\text{BTO}} \parallel [100]_{\text{Si}}$, and the longer (polar) c axis of the BTO film is oriented out-of-plane, $[001]_{\text{BTO}} \parallel [001]_{\text{Si}}$. Note that here and in the following, all crystallographic axes refer to this BTO lattice. High resolution $\theta/2\theta$ -scans around the out-of-plane and grazing incidence around the in-plane $\{200\}$ -type BTO reflections are shown in Fig. 1(b). A comparison of the two reflections shows that the average in-plane lattice parameter is shorter than the out-of-plane lattice parameter. In agreement with previous reports [7,15], this indicates that the 50-nm film is mostly c -axis-oriented BTO. We note, however, that our peak analysis of the diffraction data is compatible with a small contribution of a -oriented domains.

To investigate the influence of an in-plane electric field on the ferroelectric domain distribution in the BTO | Si heterostructure, planar capacitors were fabricated by depositing parallel tungsten electrodes on the BTO thin-film surface. The distance between the electrodes is 5 μm . The in-plane orientation of the electrode gap is varied between devices for testing the effect of in-plane electric fields along $[100]_{\text{BTO}}$, $[010]_{\text{BTO}}$, and $[110]_{\text{BTO}}$. The fabrication process has been described elsewhere [14].

III. EXPERIMENT

We investigated the ferroelectric domain configuration of the BTO film using laser-optical SHG, i.e., frequency doubling of light. This process is parameterized by the material-dependent tensor components of the second-order nonlinear susceptibility, $\chi^{(2)}$. In the electric-dipole approximation, it takes the form

$$P_i(2\omega) = \epsilon_0 \chi_{ijk}^{(2)} E_j(\omega) E_k(\omega). \quad (1)$$

Here $E_{j,k}(\omega)$ are the electric-field components of the incident fundamental beam and $P_i(2\omega)$ denotes the resulting nonlinear polarization in the material which acts as source for the emitted SHG light. Just as for the Pockels effect, the tensor nature of $\chi^{(2)}$ makes the SHG response of a ferroelectric sensitive to the orientation of the inversion-symmetry-breaking spontaneous polarization in the material, and, thus, to its ferroelectric domain state [19,20]. In contrast, scanning probe microscopy (SPM) techniques typically employed to study ferroelectric domain architectures rely on the coupling between the

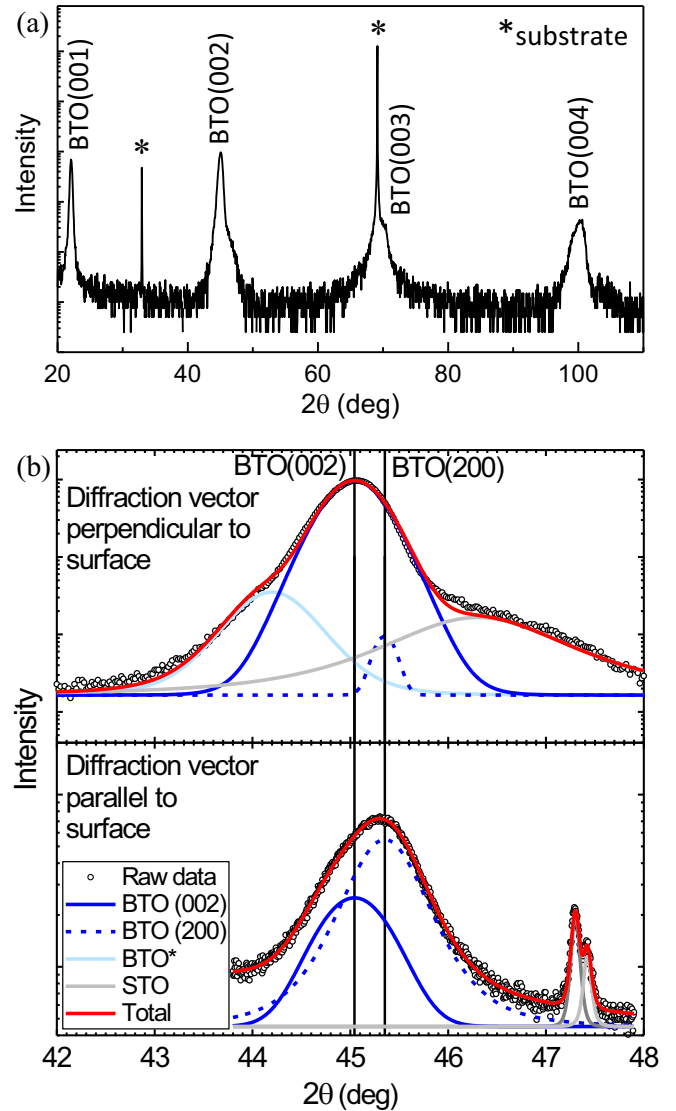


FIG. 1. (a) X-ray-diffraction $\theta/2\theta$ scan revealing a single-phase epitaxial film of tetragonal BTO on Si. (b) High-resolution $\theta/2\theta$ scan around the out-of-plane (top) and grazing incidence scan of the in-plane (bottom) $\{200\}$ -type BTO reflections. The diffraction profiles are fitted with contributions of both c -oriented and a -oriented domains. The extracted lattice parameters are $a = 0.3996$ nm and $c = 0.4022$ nm. These values slightly deviate from the bulk parameters, possibly because of tensile strain originating from the difference in the coefficient of thermal expansion between silicon and BTO. The out-of-plane diffraction profile can be fitted with a very small contribution of a -domains. For the in-plane diffraction data, the area ratio of the a -domain contribution is 30% with respect to the c -domains. The difference in a -domain contribution between the two measurement configurations suggests that, due to the grazing incidence geometry, the in-plane diffraction profile strongly overestimates the actual volume fraction of a -domains predominantly situated close to the surface. The diffraction peak analysis furthermore reveals the convolution of the BTO peaks with the diffraction peaks of the underlying STO buffer as well as the possible presence of a highly compressive strained layer of BTO at the STO interface, labeled BTO*.

polarization state and the piezoelectric response. Hence, while SPM necessitates conducting bottom electrodes for optimal response from surface domain states, SHG has the advantage of being contact-free, yet possessing the bulk sensitivity to address multidomain distributions of polar axes throughout the thickness of the film [21], even during the deposition process [22,23], in absence of electrodes [24], and when this film is integrated into a device architecture [25–27]. For tetragonal BTO, three different crystallographic domains can be defined. These correspond to six polarization states because of the possible (\pm)-orientation of the polarization with respect to the long tetragonal axis of each crystallographic domain. Ferroelectric domains whose polarization points along either of the two in-plane crystallographic directions are termed a_1 - and a_2 -domains whereas out-of-plane-polarized domains are termed c -domains, as defined in Fig. 2(a).

The $\chi^{(2)}$ tensor for tetragonal BTO is defined by its $4mm$ point-group symmetry [28]. The set of nonzero elements in this point group allows for clear separation of contributions from a_1 -, a_2 -, and c -domains in an experiment varying the direction of the wave vector of the incident light with respect to the sample orientation as described in detail in Ref. [21]. SHG measurements in normal incidence are only sensitive to a -domain contributions, yielding so-called a -SHG. By tilting the sample, SHG from c -domains (c -SHG) can also contribute to the signal. In thin-film samples, unique a -vs- c selectivity of the SHG response is most conveniently achieved in transmission geometry. However, silicon is a strong absorber in the SHG wavelength range typically employed for probing ferroelectric oxides [20,25], rendering SHG studies of domain distributions in silicon-based thin-film systems scarce. Here, we circumvent the issue of absorption by taking advantage of the near-infrared transparency of silicon and design a transmission experiment with incidence of the fundamental beam at $\lambda_{\text{fund}} = 1300$ nm onto the back of the silicon wafer [Fig. 2(b)]. Hence, the fundamental light is transmitted through the silicon to the BTO film, letting the SHG light, which would be otherwise absorbed in the substrate, directly exit our heterostructure from the surface of the BTO film.

A Ti:sapphire laser at $\lambda = 800$ nm with a pulse width of 120 fs and repetition rate of 1 kHz was converted to $\lambda_{\text{fund}} = 1300$ nm using an optical parametric amplifier. The $\chi^{(2)}$ components contributing to the SHG signal at $\lambda_{\text{SHG}} = 650$ nm were evaluated from the dependence of the SHG intensity on the light polarization of incident and detected beams. This so-called SHG anisotropy measurement was performed by rotating the polarization of the fundamental beam by the angle α between 0° and 360° and detecting the SHG light in parallel configuration under an angle $\beta = \alpha$.

The electric-field dependence of the BTO domain-distribution was investigated by applying square electric field pulses of 50 kV/cm, well above the BTO coercive field [7], for 60 s across the planar electrode pairs on top of the BTO surface. To characterize the BTO domain distribution in just the area where the electric field had been applied, i.e., within the gap between the electrode pairs, we used spatially resolved SHG imaging of the sample as described in Figs. 2(b) and 2(c), with integration times of 2 to 3 min. For domain populations where the individual domains are of suboptical-resolution size (here: $\lesssim 0.7\mu\text{m}$), as is often

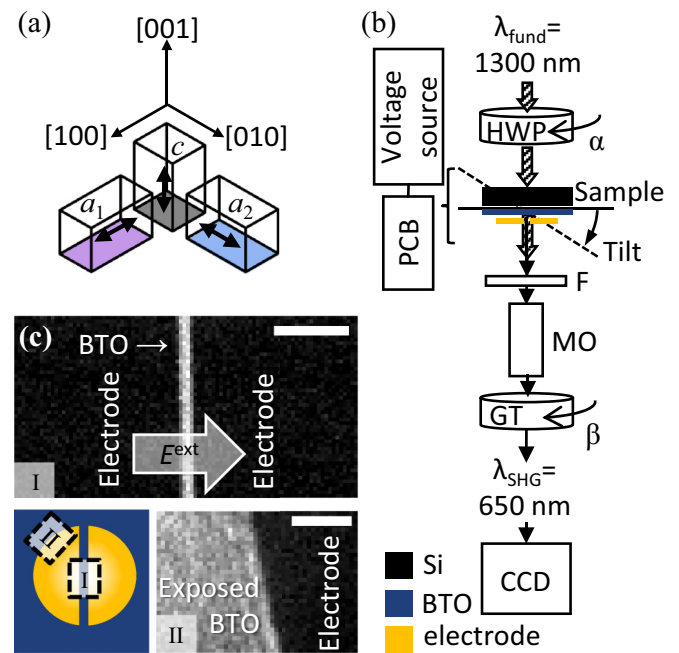


FIG. 2. (a) Schematic showing the relative orientation of a_1 -, a_2 -, and c -domains. The double-headed arrows indicate the two possible directions for the spontaneous polarization of each crystallographic domain type. (b) Top-view schematic of the experimental setup for SHG imaging in transmission geometry. The light polarization (α) of the fundamental laser beam is then set by a rotatable half-wave plate (HWP). The beam is incident on the back of the Si substrate at the angle of the sample tilt. The SHG signal is separated from the fundamental beam using a bandpass filter (F) and spatially resolved by a microscope objective (MO). The detected SHG polarization (β) is selected by a rotatable Glan-Taylor prism (GT). The resulting SHG image is acquired by a nitrogen-cooled CCD camera. For application of an in-plane electric field to the BTO | Si electro-optic devices, the electrodes are wire-bonded to a printed circuit board (PCB) and connected to a voltage source. (c) SHG images in tilted incidence of the pristine BTO film in the electrode gap (I) and next to the device (II). The corresponding positions are marked in the top-view schematic. The direction of the applied electric field is indicated by the large arrow in (I). The dark regions of the SHG images correspond to areas of the BTO covered by the patterned tungsten electrodes. The scale bars are 20 μm .

the case in thin films, the SHG light from different domain states interferes. SHG waves from domain states with parallel polarization interfere constructively, while antiparallel polarization leads to a 180° phase difference between the corresponding SHG contributions so that destructive interference occurs [22,29]. Note that although the domains in our BTO | Si heterostructure are below this resolution limit, we nevertheless obtain information on the overall domain architecture through the characteristic SHG anisotropy yielded by this domain-state interference.

IV. RESULTS

A. Pristine ferroelectric domain architecture

Figure 3(a) shows the SHG anisotropy of the pristine BTO film for normal and tilted incidence. As mentioned, only

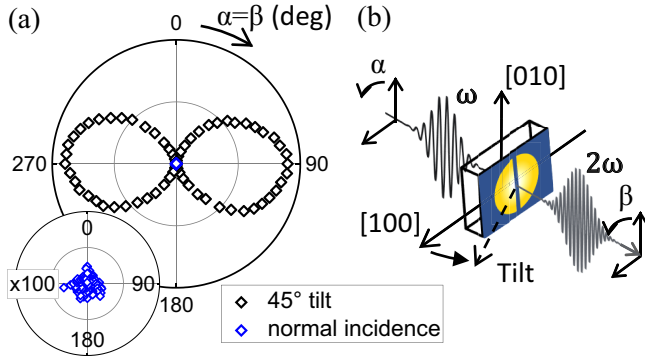


FIG. 3. (a) SHG anisotropy measurement from the pristine BTO film, at 45° sample tilt (black) and in normal incidence (blue), as a function of parallel incident and detected light polarizations, as defined in Sec. III. The inset shows a 100× magnification of the SHG anisotropy measurement in normal incidence. The absence of *a*-domain-related *a*-SHG in normal incidence indicates that the nonzero SHG signal in tilted incidence is of pure *c*-SHG type. Hence, only out-of-plane polarized *c*-domains are contributing to the SHG in the pristine state. (b) Schematic of the measurement configuration in (a). For measurements in tilted incidence, the sample is rotated around the vertical axis, corresponding to a projection of the out-of-plane [001]_{BTO}-axis onto the horizontal (90°/270°) direction.

a-SHG is allowed in normal incidence. The absence of a SHG signal in this configuration indicates that the nonzero SHG response we obtain in tilted incidence, where *a*- and *c*-SHG are mixed, is of pure *c*-SHG type. Hence, only the ferroelectric polarization of *c*-domains contributes to the net SHG response in the pristine BTO film. The anisotropy of this *c*-SHG signal corresponds to a double lobe pointing along the planar projection of the out-of-plane polar axis (along 90°/270°), which, in the present case, coincides with the horizontal direction of the sample tilt, as defined in Fig. 3(b). Note that the SHG intensity reaches zero for a light polarization perpendicular to the polar axis (0°/180° in Fig. 3), a property we will make use of later on. The SHG anisotropy for the pristine BTO was measured both on the exposed film next to the devices and in the small slit between the electrodes [see Fig. 2(c)]. In both cases, identical SHG polarization anisotropies were obtained with only an overall difference in intensity. This confirms that our SHG probe technique resolves well the small area of BTO serving as active device region.

Even though we observe absence of an *a*-domain contribution in the SHG signal from the as-grown thin film and even though XRD analysis indicates a predominantly *c*-oriented film (Fig. 1), intermixed *a*- and *c*-domains have been previously reported for BTO films as thin as 8 nm on silicon substrates [15]. Our BTO film at 50 nm exceeds this thickness by far. We therefore conclude that the absence of *a*-SHG indicates either (i) a density of *a*-domains below the experimental detection threshold or (ii) complete cancellation of destructively interfering SHG contributions from *a*-domains smaller than the optical resolution limit with equal volume fractions of antiparallel polarization domain states. In the following, we will see that, not only are we able to discriminate between these two cases, but we also provide

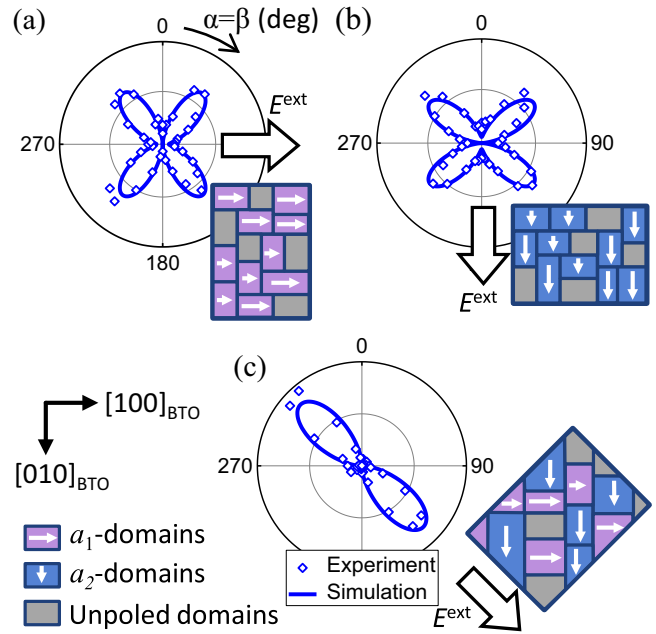


FIG. 4. (a)–(c) SHG anisotropy in normal incidence for the 50-nm BTO film subsequent to in-plane poling along (a) [100]_{BTO}, (b) [010]_{BTO}, and (c) [110]_{BTO}. The solid lines are SHG anisotropy simulations using BTO bulk coefficients of $\chi^{(2)}$ and assuming the domain architecture sketched in the respective insets.

insight into the type of domain reorientation triggered upon electrical poling.

B. Electric poling of *a*-domains

To scrutinize the ferroelectric domain distribution in the 50-nm BTO layer and its response to electrical poling, we used SHG imaging in combination with electric-field application along the plane of the film, as described in Sec. III. Poling was investigated in three device configurations, namely, electric field along [100]_{BTO}, [010]_{BTO}, and [110]_{BTO}. The normal-incidence *a*-SHG anisotropies after in-plane electrical poling are shown for each of these configurations in Figs. 4(a)–4(c). While measurements in the pristine state, as discussed in Sec. IV A, did not yield any *a*-SHG, application of the in-plane electric field led to a remanent *a*-SHG signal in the gap between the electrodes. This signal was more than 30 times larger than the detection threshold of SHG, clearly evidencing electric-field poling of *a*-domains for all device configurations. SHG measurements on BTO films as thin as 26 nm on silicon reveal a similar presence of *a*-SHG that appears only after in-plane electric-field application. We can understand the poling-induced presence of *a*-SHG by comparing the experimental data in Figs. 4(a)–4(c) with SHG anisotropy simulations of different *a*₁- and *a*₂-domain configurations using bulk BTO values [30] for the tensor components of $\chi^{(2)}$ in Eq. (1). We find agreement between theory and experiment when assuming that the electric field along [100]_{BTO} only generates a poled *a*₁-domain population [Fig. 4(a)], whereas the electric field along [010]_{BTO} poles only an *a*₂-domain population [Fig. 4(b)]. Hence, the two

cases are identical up to a 90° in-plane rotation. With an electric field along $[110]_{\text{BTO}}$, equal fractions of the two a -domain types are poled, leading to a fundamental change in the SHG anisotropy [Fig. 4(c)] that corresponds to the coherent superposition of the a_1 and a_2 cases described above. Thus, we see that the in-plane electric field yields a poled a -domain architecture, where the relative field components along the principal crystallographic a axes control the poling ratio of the two in-plane domain variants. To gain a full understanding of the domain dynamics in the system, however, it is necessary to also determine the type of domain architecture in the pristine film that forms the reservoir out of which these a -domains are electrically coerced.

For this purpose, we consider two scenarios for the electric-field alignment of a -domains, following the two cases discussed in Sec. IV A. First we consider a reorientation of c -domains into a -domains in the absence of an as-grown a -domain reservoir to draw from [case (i)]. For example, previous studies have shown c - to a -domain reorientation by electrical poling in both BTO bulk crystals [31] and $\text{Pb}(\text{Zr}_{0.2}\text{Ti}_{0.8})\text{O}_3$ (PZT) thin films [32,33]. Alternatively, the generation of a -domains could result from poling of a pre-existing, 1:1 population of oppositely polarized a -domains [case (ii)].

For case (i), the ferroelastic transformation of domains from c - to a -axis orientation would manifest itself as an increase in a -SHG intensity with a corresponding decrease of c -SHG intensity, as the a -domain population would grow at the expense of the c -domain population. For case (ii), on the other hand, the onset of a -SHG from the poling of pre-existing a_1 - or a_2 -domains would leave the c -SHG contribution constant, as the c -domain population itself would remain unchanged.

C. Electric-field dependence of c -domain population

Independent access to both a - and c -SHG contributions in thin-film ferroelectrics has previously been achieved by performing a set of subsequent measurements in different optical configurations. However, investigation of the actual poling mechanism requires an *operando* approach with simultaneous access to the two SHG contributions during poling within a single experimental setup. In the previous section, all SHG measurements were performed in normal incidence where only a -SHG can contribute to the SHG signal. To allow all SHG contributions, we now turn to a tilted-incidence SHG geometry [Fig. 5(a)]. We used the $[110]_{\text{BTO}}$ -oriented device for this type of experiment. In contrast to the $[100]_{\text{BTO}}$ - and $[010]_{\text{BTO}}$ -oriented device types, here the a -SHG anisotropy exhibits a double-lobe symmetry where the SHG contribution peaks along the electric-field and net-polarization direction but is zero perpendicular to it [see Fig. 4(c)]. Similarly, as seen in Fig. 3, the c -SHG exhibits a double-lobe anisotropy which is maximized along the projection of the out-of-plane polar axis onto the direction of the sample tilt (along $90^\circ/270^\circ$), and is zero perpendicular to it. Thus, by tilting the sample and orienting it such that $[110]_{\text{BTO}}$ ($\parallel E^{\text{ext}}$) is perpendicular to the horizontal sample tilt, a -SHG and c -SHG are polarized orthogonal to each other [see schematic in Fig. 5(b)]. This enables simultaneous and cross-interference-free detection of both contributions.

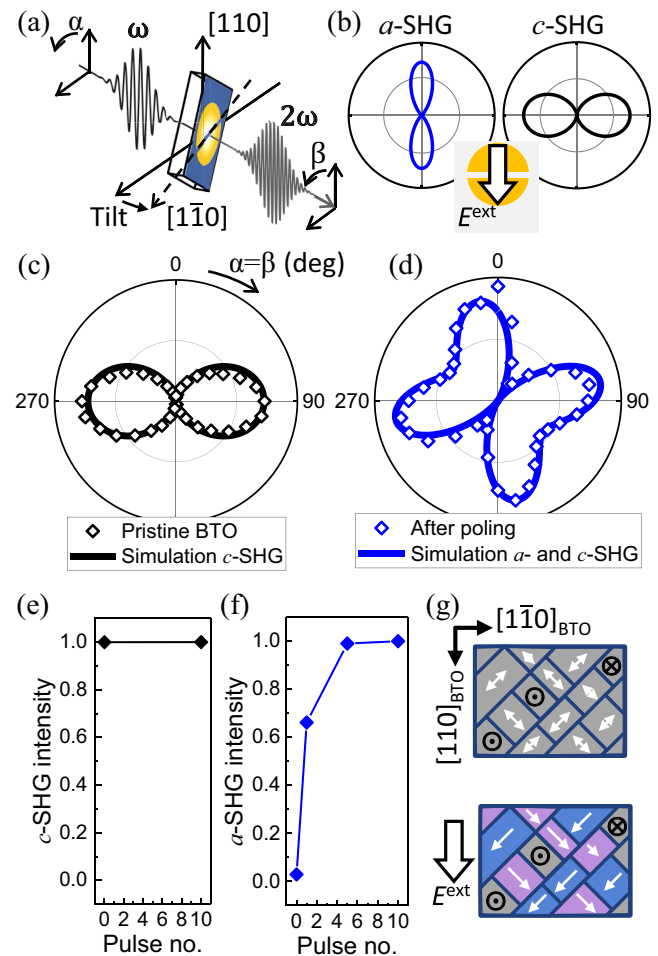


FIG. 5. Independent characterization of a - and c -SHG on BTO thin films in tilted incidence. (a) Schematic of the measurement geometry. (b) Expected a - and c -SHG anisotropies after poling along $[110]_{\text{BTO}}$ in the measurement geometry in (a) with a 30° sample tilt. (c), (d) SHG anisotropy before (c) and after (d) in-plane poling of the BTO film. The solid lines show corresponding SHG simulations using bulk values for $\chi^{(2)}$, given the domain architectures sketched in (g). (e), (f) Evolution of the c -SHG (e) and a -SHG (f) intensity as function of the number of applied electric-field pulses (maximum $\equiv 1$). (g) Sketch of the domain architecture in the pristine BTO film (top) and the same film subsequent to in-plane electrical poling (bottom). Only preexisting a -domains that in the pristine state lack a net polarization direction are poled. The a_1 - and a_2 -domains are poled in equal fractions, indicated by purple and blue, respectively. The c -domain population remains unchanged during in-plane poling.

In this tilted-incidence configuration, we measured the evolution of the SHG anisotropy [Figs. 5(c) and 5(d)] and SHG intensity [Figs. 5(e) and 5(f)] following the application of consecutive voltage pulses to the $[110]_{\text{BTO}}$ -oriented device. As noted earlier, only c -SHG is detected for the pristine state before poling [Fig. 5(c)]. Directly after the first voltage pulse, a drastic change in the anisotropy of the SHG signal was observed [Fig. 5(d)]. The a -domain population induced by the poling leads to the onset of a -SHG that appears perpendicular to the c -SHG signal, as detailed above. Given the 30° sample tilt and assuming an initially homogeneously polarized

c-oriented matrix, the SHG simulations [34] provide an estimation of the upper limit for the relative volume fraction of *a*-domains after poling of 34%. Allowing instead a mixed domain configuration rather than a single domain state for the *c*-domain matrix will, however, yield a lower volume fraction of *a*-domains [35], in agreement with the XRD analysis.

Notably, the sudden increase in *a*-SHG was not accompanied by any significant change in the *c*-SHG intensity [Fig. 5(e)]. As seen in Fig. 5(f), the *a*-SHG intensity is fully saturated after five pulses; after applying another five pulses, no further change of either *a*- nor *c*-SHG yields was observed. Furthermore, back switching was not detected; the poled *a*-domain state exhibits long-term remanence.

We recall that a *c*- to *a*-domain reorientation as discussed earlier in case (i) would be expected to lead to a reduction in the *c*-SHG intensity when going from pristine to fully poled state. Clearly, the conservation of the *c*-domain population during in-plane poling in combination with the saturation of the *a*-SHG response is in stark contrast to this scenario and thus excludes such ferroelastic *c*- to *a*-domain reorientation in the BTO heterostructure. Therefore, the reservoir for the poled *a*-domains related to the emerging *a*-SHG signal must be a preexisting *a*-domain population, which in the pristine state consists of equal volume fractions of antiparallel polarization directions, corresponding to case (ii) above and sketched in Fig. 5(g).

V. DISCUSSION

By probing the ferroelectric domain distribution in BTO thin-films integrated on silicon with noninvasive laser-optical SHG, we could clearly distinguish between *c*- and *a*-domain populations and thus monitor their individual response to an external, in-plane-oriented electric field. We characterized this poling behavior directly in the integrated device architecture. The subresolution domain size of the ferroelectric *a*-domain population precluded its detection in the pristine BTO film (a common issue for ultrathin ferroelectric films), yet here we accessed it by aligning the *a*-domains along the in-plane electric field, uncovering a multidomain state for the pristine BTO film. The in-plane electric field acts exclusively on the *a*-domain populations, leaving the *c*-domain population intact for electric fields up to at least 50 kV/cm. We thus excluded the occurrence of (irreversible) ferroelastic *c*- to

a-domain reorientation in the BTO thin films. This stands in contrast to reports on domain reorientation in PZT thin films [32,33] and may be attributed to the stronger coupling between strain and electric dipoles in the BTO thin films compared to PZT, where local rotation of polarization is more frequently observed [36]. We have further shown that the ratio between poled *a*₁- and *a*₂-domain populations can be controlled by the choice of in-plane direction of the applied electric field. Conversely, the *c*-domain population can be individually accessed by an out-of-plane oriented field, as has been reported for similar BTO | Si heterostructures even in the absence of a bottom electrode [15]. These nonmixing *a*- and *c*-domain populations that can be individually addressed by the choice of the orientation of the applied electric field thus indicate the possibility of multilevel control of electro-optic response in BTO-based integrated photonic devices. Therefore, we expect our work to stimulate further investigations of oxide heterostructures taking advantage of mixed in-plane and out-of-plane anisotropies.

ACKNOWLEDGMENTS

J. Nordlander, M.T., and M.F. acknowledge financial support by the EU European Research Council under Advanced Grant Program No. 694955-INSEETO and the Swiss National Science Foundation under Project No. 200021_178825. M.R. and A.A.D. gratefully acknowledge support by the National Science Foundation under Grant No. IRES-1358111 and by the Air Force Office of Scientific Research under Grant No. FA9550-18-1-0053. F.E., D.C., S.A., and J.F. acknowledge funding from the European Commission under the Grants Agreement No. H2020-ICT-2015-25-688579 (PHRESCO) and No. H2020-ICT-2017-1-780997 (plaCMOS), and from the Swiss State Secretariat for Education, Research and Innovation under Contracts No. 15.0285 and No. 16.0001, and from the Swiss National Foundation Project No. 200021_159565 (PADOMO).

All authors discussed the results and contributed to the completion of the paper. F.E., D.C., S.A., and J.F. performed the thin film growth, electrode patterning, and structural analysis. J. Nordlander coordinated the SHG measurements and developed the SHG simulation model with F.E., M.R., J. Nürnberg, G.D.L., M.F., and M.T.

M.T., J. Nordlander, S.A., J.F., and M.F. designed the experiment and supervised the work jointly with A.A.D.

-
- [1] N. Setter, D. Damjanovic, L. Eng, G. Fox, S. Gevorgian, S. Hong, A. Kingon, H. Kohlstedt, N. Y. Park, G. B. Stephenson, I. Stolitchnov, A. K. TagansteV, D. V. Taylor, T. Yamada, and S. Streiffner, *J. Appl. Phys.* **100**, 051606 (2006).
 - [2] J. F. Scott, *Science* **315**, 954 (2007).
 - [3] E. L. Wooten, K. M. Kissa, A. Yi-Yan, E. J. Murphy, D. A. Lafaw, P. F. Hallemeier, D. Maack, D. V. Attanasio, D. J. Fritz, G. J. McBrien, and D. E. Bossi, *IEEE J. Sel. Top. Quantum Electron.* **6**, 69 (2000).
 - [4] A. Politi, J. C. Matthews, M. G. Thompson, and J. L. O'Brien, *IEEE J. Sel. Top. Quantum Electron.* **15**, 1673 (2009).
 - [5] C. Xiong, W. H. Pernice, J. H. Ngai, J. W. Reiner, D. Kumah, F. J. Walker, C. H. Ahn, and H. X. Tang, *Nano Lett.* **14**, 1419 (2014).
 - [6] S. Abel, F. Eltes, J. E. Ortmann, A. Messner, P. Castera, T. Wagner, D. Urbonas, A. Rosa, A. M. Gutierrez, D. Tulli, P. Ma, B. Baeuerle, A. Josten, W. Heni, D. Caimi, L. Czornomaz, A. A. Demkov, J. Leuthold, P. Sanchis, and J. Fompeyrine, *Nat. Mater.* **18**, 42 (2019).
 - [7] S. Abel, T. Stöferle, C. Marchiori, C. Rossel, M. D. Rossell, R. Erni, D. Caimi, M. Sousa, A. Chelnokov, B. J. Offrein, and J. Fompeyrine, *Nat. Commun.* **4**, 1671 (2013).

- [8] F. Eltes, C. Mai, D. Caimi, M. Kroh, Y. Popoff, G. Winzer, D. Petousi, S. Lischke, J. E. Ortman, L. Czornomaz, L. Zimmermann, J. Fompeyrine, and S. Abel, *J. Light. Technol.* **37**, 1456 (2019).
- [9] J. Wang, F. Sciarrino, A. Laing, and M. G. Thompson, *Nat. Photonics* (2019), doi:10.1038/s41566-019-0532-1.
- [10] J. Lyu, I. Fina, R. Solanas, J. Fontcuberta, and F. Sánchez, *Sci. Rep.* **8**, 495 (2018).
- [11] M. Scigaj, C. H. Chao, J. Gázquez, I. Fina, R. Moalla, G. Saint-Girons, M. F. Chisholm, G. Herranz, J. Fontcuberta, R. Bachelet, and F. Sánchez, *Appl. Phys. Lett.* **109**, 122903 (2016).
- [12] M. Scigaj, N. Dix, J. Gázquez, M. Varela, I. Fina, N. Domingo, G. Herranz, V. Skumryev, J. Fontcuberta, and F. Sánchez, *Sci. Rep.* **6**, 31870 (2016).
- [13] Y. L. Li and L. Q. Chen, *Appl. Phys. Lett.* **88**, 072905 (2006).
- [14] K. J. Kormondy, Y. Popoff, M. Sousa, F. Eltes, D. Caimi, M. D. Rossell, M. Fiebig, P. Hoffmann, C. Marchiori, M. Reinke, M. Trassin, A. A. Demkov, J. Fompeyrine, and S. Abel, *Nanotechnology* **28**, 075706 (2017).
- [15] C. Dubourdieu, J. Bruley, T. M. Arruda, A. Posadas, J. Jordan-Sweet, M. M. Frank, E. Cartier, D. J. Frank, S. V. Kalinin, A. A. Demkov, and V. Narayanan, *Nat. Nanotechnol.* **8**, 748 (2013).
- [16] Z. Li, X. Guo, H.-B. Lu, Z. Zhang, D. Song, S. Cheng, M. Bosman, J. Zhu, Z. Dong, and W. Zhu, *Adv. Mater.* **26**, 7185 (2014).
- [17] R. Guo, Z. Wang, S. Zeng, K. Han, L. Huang, D. G. Schlom, T. Venkatesan, Ariando, and J. Chen, *Sci. Rep.* **5**, 12576 (2015).
- [18] S. M. Yang, A. N. Morozovska, R. Kumar, E. A. Eliseev, Y. Cao, L. Mazet, N. Balke, S. Jesse, R. K. Vasudevan, C. Dubourdieu, and S. V. Kalinin, *Nat. Phys.* **13**, 812 (2017).
- [19] M. Fiebig, V. V. Pavlov, and R. V. Pisarev, *J. Opt. Soc. Am. B* **22**, 96 (2005).
- [20] S. A. Denev, T. T. A. Lummen, E. Barnes, A. Kumar, and V. Gopalan, *J. Am. Ceram. Soc.* **94**, 2699 (2011).
- [21] G. De Luca, M. D. Rossell, J. Schaab, N. Viart, M. Fiebig, and M. Trassin, *Adv. Mater.* **29**, 1605145 (2017).
- [22] G. De Luca, N. Strkalj, S. Manz, C. Bouillet, M. Fiebig, and M. Trassin, *Nat. Commun.* **8**, 1419 (2017).
- [23] N. Strkalj, G. De Luca, M. Campanini, S. Pal, J. Schaab, C. Gattinoni, N. A. Spaldin, M. D. Rossell, M. Fiebig, and M. Trassin, *Phys. Rev. Lett.* **123**, 147601 (2019).
- [24] J. Nordlander, M. Campanini, M. D. Rossell, R. P. Erni, Q. N. Meier, A. Cano, N. A. Spaldin, M. Fiebig, and M. Trassin, *Nat. Commun.* **10**, 5591 (2019).
- [25] J. Nordlander, G. De Luca, N. Strkalj, M. Fiebig, and M. Trassin, *Appl. Sci.* **8**, 570 (2018).
- [26] G. De Luca, P. Schoenherr, J. Mendil, D. Meier, M. Fiebig, and M. Trassin, *Phys. Rev. Appl.* **10**, 054030 (2018).
- [27] N. Strkalj, E. Gradauskaitė, J. Nordlander, and M. Trassin, *Materials* **12**, 3108 (2019).
- [28] R. R. Birss, *Symmetry and Magnetism*, Vol. 863 (North-Holland Pub. Co., Amsterdam, 1964).
- [29] H. Yokota, J. Kaneshiro, and Y. Uesu, *Phys. Res. Int.* **2012**, 704634 (2012).
- [30] Y. Shen, *The Principles of Nonlinear Optics*, Wiley Classics Library (Wiley-Interscience, Hoboken, NJ, 2003).
- [31] T. H. E. Lahtinen, K. J. A. Franke, and S. van Dijken, *Sci. Rep.* **2**, 258 (2012).
- [32] A. I. Khan, X. Marti, C. Serrao, R. Ramesh, and S. Salahuddin, *Nano Lett.* **15**, 2229 (2015).
- [33] P. Gao, J. Britson, C. T. Nelson, J. R. Jokisaari, C. Duan, M. Trassin, S.-H. Baek, H. Guo, L. Li, Y. Wang, Y.-H. Chu, A. M. Minor, C.-B. Eom, R. Ramesh, L.-Q. Chen, and X. Pan, *Nat. Commun.* **5**, 3801 (2014).
- [34] Our simulations, using bulk BTO values for $\chi^{(2)}$, indicate relative SHG contributions $a_1 : a_2 : c = 0 : 0 : 1$ before poling, and $a_1 : a_2 : c = 0.255 : 0.255 : 1$ after poling.
- [35] The estimated volume fraction of a -domains is relative to the total c -SHG yield. The presence of c -domains of either orientation would reduce the c -SHG yield because of destructive interference between SHG contributions from P_{up} and P_{down} .
- [36] B.-K. Lai, I. Ponomareva, I. A. Kornev, L. Bellaiche, and G. J. Salamo, *Phys. Rev. B* **75**, 085412 (2007).